International Journal of Heat and Fluid Flow 49 (2014) 43–52

Contents lists available at ScienceDirect

International Journal of Heat and Fluid Flow

journal homepage: www.elsevier.com/locate/ijhff

Turbulent thermal boundary layers with temperature-dependent viscosity

Jin Lee [a], Seo Yoon Jung [b,1], Hyung Jin Sung [a,*], Tamer A. Zaki [b,2]

[a] Department of Mechanical Engineering, KAIST, 291 Daehak-ro, Yuseong-gu, Daejeon 305-701, Republic of Korea
[b] Department of Mechanical Engineering, Imperial College London, South Kensington Campus, London SW7 2AZ, UK

ARTICLE INFO

Article history:
Available online 1 May 2014

Keywords:
Direct numerical simulation
Turbulent boundary layer
Temperature-dependent viscosity
Scalar transport

ABSTRACT

Direct numerical simulations (DNS) of turbulent boundary layers (TBLs) over isothermally heated walls were performed, and the influence of the wall-heating on the thermal boundary layers was investigated. The DNS adopt an empirical relation for the temperature-dependent viscosity of water. The Prandtl number therefore changes with temperature, while the Péclet number is constant. Two wall temperatures (T_w = 70 °C and 99 °C) were considered relative to T_∞ = 30 °C, and a reference simulation of TBL with constant viscosity was also performed for comparison. In the variable viscosity flow, the mean and variance of the scalar, when normalized by the friction temperature deficit, decrease relative to the constant viscosity flow. A relation for the mean scalar which takes into account the variable viscosity is proposed. Appropriate scalings for the scalar fluctuations and the scalar flux are also introduced, and are shown to be applicable for both variable and constant viscosity flows. Due to the modification of the near-wall turbulence, the Stanton number and the Reynolds analogy factor are augmented by 10% and 44%, respectively, in the variable viscosity flow. An identity for the Stanton number is derived and shows that the mean wall-normal velocity and wall-normal scalar flux cause the increase in the heat transfer coefficient. Finally, the augmented near-wall velocity fluctuations lead to an increase of the wall-normal scalar flux, which contributes favorably to the enhanced heat transfer at the wall.

1. Introduction

Turbulent flows of liquids over heated walls are of practical importance in many engineering problems such as heat exchangers and nuclear reactors. For common liquids including water, viscosity decreases with increasing temperature. When a large temperature difference between the wall and the free stream is established, the resulting temperature gradient near the wall causes a gradual change in viscosity. Although turbulence modification due to the temperature-dependent viscosity in heated flows was previously addressed (e.g. Zonta et al., 2012; Lee et al., 2013), the effect of the viscosity variation on the thermal boundary layer and scalar transport has not received a similar level of attention.

A number of studies were devoted to numerical simulations of turbulent thermal boundary layer flows, but have generally assumed constant fluid properties and in particular the Prandtl number, *Pr*. For example, based on direct numerical simulations (DNS), Kong et al. (2000) demonstrated the similarity between the wall-normal heat flux and the Reynolds stresses, which underlies the correlation between the temperature and the streamwise velocity fluctuations. Most of the earlier studies concentrated on the effect of different, but constant, *Pr* on the mean scalar quantities and scalar fluxes. Tiselj et al. (2001) and Kozuka et al. (2009) investigated scalar transfer in turbulent channel flows at different Prandtl numbers. Abe et al. (2004) examined the Reynolds-number (*Re*) effect on the scalar transfer as well as the *Pr*-effect (Pr = 0.71 and 0.025) in channel flows. They showed that the scalar-flux fluctuations are increased in high-*Re* flows due to augmented turbulence activity. Transitional and turbulent thermal boundary layers were studied by Li et al. (2009) and Wu and Moin (2010). The former work investigated the effects of thermal boundary conditions and the Prandtl number. Wu and Moin (2010) provided the statistics of a spatially developing flow up to relatively higher-*Re*. These studies focused on the scalar transport and contributed to our understanding of turbulence structures including the velocity and temperature fluctuations in flows with various thermal boundary conditions and Prandtl numbers.

* Corresponding author. Tel.: +82 42 350 3027; fax: +82 42 350 5027.
E-mail address: hjsung@kaist.ac.kr (H.J. Sung).

[1] Present address: Advanced Reactor Development Institute, KAERI, 989-111, Daedeok-daero, Yuseong-gu, Daejeon 305-353, Republic of Korea.

[2] Present address: Department of Mechanical Engineering, Johns Hopkins University, Baltimore, MD 21218, USA.

http://dx.doi.org/10.1016/j.ijheatfluidflow.2014.04.004
0142-727X/

The above numerical studies assumed constant fluid viscosity or, equivalently, Prandtl number. Few researchers took into account the temperature-dependence of viscosity, e.g. Wall and Wilson (1997) and Sameen and Govindarajan (2007). Most previous research on the influence of viscosity stratification focused on the stability of laminar boundary layers and not on TBLs. We herein address this gap and consider the case of temperature-dependent viscosity, where the Prandtl number varies spatially within the TBL. One relevant study was the recent work by Zonta et al. (2012), who performed DNS of turbulent channel flow with wall heating. They examined the effect of inhomogeneous viscosity and found that turbulence production and dissipation of the wall-bounded flow were significantly altered. Their work did not, however, consider the heating of spatially developing flows.

Recently, the mechanism of skin-friction reduction owing to the temperature-dependent viscosity was studied by Lee et al. (2013). That work demonstrated weakening of the outer vortices and enhanced fine-scale motions near the heated walls. The present work is a continuation of the study by Lee et al. (2013). We examine the transport of scalars, such as temperature or concentration, owing to the viscosity gradient. DNS data of forced convection in TBLs with temperature-dependent viscosity are utilized. The free-stream fluid is assumed to be water at 30 °C, which corresponds to $Pr = 5.4$. Using an empirical model of the water viscosity, two wall temperatures (70 °C and 99 °C) are considered in order to establish the viscosity difference; namely, moderately heated (MH) and strongly heated (SH) walls. For comparison, a conventional passive scalar simulation, herein referred to as constant viscosity (UH; the term was 'unheated' in Lee et al., 2013), is also considered.

2. Numerical details

The temperature-dependent viscosity of water is defined by the Arrhenius-type viscosity model (White, 2006). In order to isolate the effect of the viscosity variation alone, the thermal diffusivity (α) and density (ρ) are assumed to be constant and are set by the free-stream temperature. The present simulation belongs to the forced convection regime, $Gr/Re^2 \ll 1$, where Gr is the Grashof number and Re is the Reynolds number.

The governing equations for an incompressible flow with temperature-dependent viscosity are

$$\frac{\partial u_i}{\partial x_i} = 0, \tag{1}$$

$$\frac{\partial u_i}{\partial t} + u_j \frac{\partial u_i}{\partial x_j} = -\frac{\partial p}{\partial x_i} + \frac{1}{Re_{\theta_{in}}} \frac{\partial}{\partial x_j}\left[\nu_R \left(\frac{\partial u_i}{\partial x_j} + \frac{\partial u_j}{\partial x_i}\right)\right], \tag{2}$$

and

$$\frac{\partial \Theta}{\partial t} + u_j \frac{\partial \Theta}{\partial x_j} = \frac{1}{Re_{\theta_{in}} Pr_\infty} \frac{\partial^2 \Theta}{\partial x_j^2}. \tag{3}$$

The velocity components in the streamwise (x), wall-normal (y) and spanwise (z) directions are u, v and w, respectively, and p is the kinematic pressure. The non-dimensional temperature deficit, herein referred to as the scalar, is defined as $\Theta = (T - T_w)/(T_\infty - T_w)$. Subscripts w and ∞ denote variables at the wall and in the free stream, respectively. The ratio of the local to the free-stream viscosity is $\nu_R \equiv \nu(T)/\nu_\infty$. Note that the physical temperature (T) is used to determine the viscosity ratio. The Reynolds and Prandtl numbers in the governing equations are $Re_{\theta_{in}}$ ($\equiv U_\infty \theta_{in}/\nu_\infty$) = 1240 and Pr_∞ ($\equiv \nu_\infty/\alpha$) = 5.4, respectively. The numerical method for the solution of the Navier-Stokes equations is summarized in Zaki et al. (2010), and was previously applied in the DNSs of various transitional (Zaki, 2013; Nolan and Zaki, 2013) and fully-turbulent flows (Lee et al., 2013).

The parameters of the main simulations are summarized in Table 1. In the heated cases, the wall temperature was set to the desired value immediately downstream of the inlet. The fluid viscosity at the heated wall is 49.7% and 35.2% of the free-steam value in the MH and SH cases, respectively. The computational domain is a rectangular region with dimensions $L_x = 400\theta_{in}$, $L_y = 60\theta_{in}$ and $L_z = 80\theta_{in}$. The number of grid points is $4097 \times 385 \times 1281$ in x, y, and z, respectively. A non-uniform grid distribution was adopted in the wall-normal direction, whereas uniform grid spacing was used in the streamwise and spanwise directions. The grid spacing in the present study is summarized in Table 2 using wall units, and in Table 3 based on the Batchelor scale. Starting from the inlet Reynolds number $Re_\theta = 1240$, the reference unheated flow reaches $Re_\theta = 2060$ at the end of the streamwise domain. The total time for statistical averaging during the DNS is $1800\theta_{in}/U_\infty$ time units.

Due to the viscosity variation with temperature, an effective Reynolds number Re_θ^{eff} is defined:

$$Re_\theta^{eff} = \frac{U_\infty \theta}{\nu^{eff}}, \tag{4}$$

where

$$\nu^{eff} = \frac{1}{\delta} \int_0^\delta \bar{\nu}(y) dy. \tag{5}$$

All results are compared at the same Re_θ^{eff}. Because an appropriate inner length-scale is required in the presence of the non-uniform fluid viscosity, the ratio of the local viscosity to the friction velocity is used, i.e. $l_\nu(y) = \bar{\nu}(y)/u_\tau$, where the friction velocity u_τ is defined using the viscosity at the wall. Therefore, the modified inner scaling is given by $y_\nu^+ \equiv y/l_\nu(y)$.

Table 1
Summary of simulation parameters. The quantities $\nu_R|_w$ and $Pr(y)$ are determined at $Re_\theta^{e}\!ff = 1840$. Note that the unheated (UH) case by Lee et al. (2013) corresponds to constant viscosity.

	T_w (°C)	T_∞ (°C)	$\nu_R\vert_w$	$Pr(y)$	Δt (Θ_{in}/U_∞)
Constant viscosity (UH)	–	–	1.000	5.4	0.025
Moderately heated (MH)	70	30	0.497	2.68–5.4	0.018
Strongly heated (SH)	99	30	0.352	1.90–5.4	0.015

Table 2
Spatial and temporal resolutions normalized by wall units.

	Δx^+	Δy^+_{min}	Δy^+_{max}	Δz^+	Δt^+
Constant viscosity (UH)	5.08	0.246	24.6	3.25	0.0564
Moderately heated (MH)	9.22	0.447	22.4	5.90	0.0670
Strongly heated (SH)	12.2	0.593	21.1	7.82	0.0698

Table 3
Spatial and temporal resolutions normalized by the Batchelor scale ($\eta_\Theta = \eta\sqrt{1/Pr}$). Subscript δ denotes the value at the free-stream edge of the momentum boundary layer.

	$(\Delta x/\eta_\Theta)_{max}$	$(\Delta y/\eta_\Theta)_{max,w}$	$(\Delta y/\eta_\Theta)_{max,\delta}$	$(\Delta z/\eta_\Theta)_{max}$
Constant viscosity (UH)	8.3	0.402	3.04	5.31
Moderately heated (MH)	11.0	0.531	3.01	7.01
Strongly heated (SH)	12.4	0.599	2.98	7.91

3. Results

The local decrease in the near-wall viscosity leads to a dramatic change in the near-wall turbulence. As shown in Fig. 1a, the skin-friction coefficient ($C_f \equiv 2\tau_w/\rho U_\infty^2$; τ_w is the local wall shear stress) is decreased appreciably. The mechanism of the skin-friction reduction due to wall heating with temperature-dependent viscosity was explained by Lee et al. (2013). Their work showed that the reduction of Reynolds shear stress in the outer region is the main factor. Fig. 1a also shows an increase in the Stanton number (St) for wall heating. Here, St is the non-dimensional heat (scalar) transfer coefficient,

$$St = \frac{q_w}{\rho U_\infty c_p(\Theta_w - \Theta_\infty)}. \tag{6}$$

The variables q_w and c_p are the rate of heat transfer from the wall to the flow and the specific heat, respectively. The Stanton number of the SH case is 10.4% higher than that of the UH case at $Re_\theta^{eff} = 1840$, even though the viscosity variation does not appear in the energy equation, i.e. the Péclet number ($Pe \equiv RePr$) is constant. Owing to the combined effect of decreased skin-friction and increased Stanton number, the Reynolds analogy factor ($2St/C_f$) of the SH case is 44.2% higher than that of the UH flow. In particular, the factor increases from 0.526 (UH) to 0.759 (SH), at $Re_\theta^{eff} = 1840$ (Fig. 1b). In Section 3.1, we examine the effect of the viscosity variation on statistics of the scalar field and, in Section 3.2, we discuss the scalar transport and the scalar flux budget in detail.

3.1. Statistics of the scalar field

3.1.1. Mean scalar

The wall-normal distribution of mean scalar is shown in Fig. 2, normalized by the friction temperature $\left(\Theta_\tau \equiv \frac{q_w}{\rho c_p u_\tau}\right)$ at $Re_\theta^{eff} = 1840$. The profile from the constant viscosity case (UH) is in good agreement with that of low-Re channel flow (Kawamura et al., 1998). The profile of the mean scalar is shifted down for the moderately and strongly heated (MH and SH) flows. As the viscosity decreases near the heated walls, the mean scalar is reduced due to the decreased Prandtl number. Note that the Prandtl number varies in a thin thermal layer relative to the momentum boundary layer. However, the mean scalar decreases to a significant extent in the outer region. This decrease is caused by the large friction temperature. The law-of-the-wall with the local Prandtl number ($\bar{\Theta}^+ = Pr(y_v)y_v^+$) and the log-law with the inclination angle of 2.12 (Kader, 1981) are plotted in Fig. 2, and both curves are in good agreement with the experimental data by Kawamura et al. (1998). If we employ the modified wall-normal coordinate y_v as the abscissa, the wall layer is divided into two regions: the conductive sublayer ($y_v^+ \simeq 5$) and the logarithmic region. The wall-normal elevations of the log-law are β = 33.3, 27.3 and 24.4 for the UH, MH and SH cases, respectively. The structure of the scalar fields in the presence of temperature-dependent viscosity is qualitatively similar to that of the passive scalar simulation (UH), although the wall-normal distribution is changed.

The mean scalar equation suggested by Kader (1981) provides a unified relation in the conductive sublayer and in the logarithmic region, given by

$$\bar{\Theta}^+ = \underbrace{Pr\ y^+ \exp(-\Gamma)}_{\text{inner}} + \underbrace{\left(2.12 \ln\left((1+y^+)\frac{2.5(2-y/\delta)}{1+4(1-y/\delta)^2}\right) + \beta(Pr)\right)\exp(-1/\Gamma)}_{\text{outer}}, \tag{7}$$

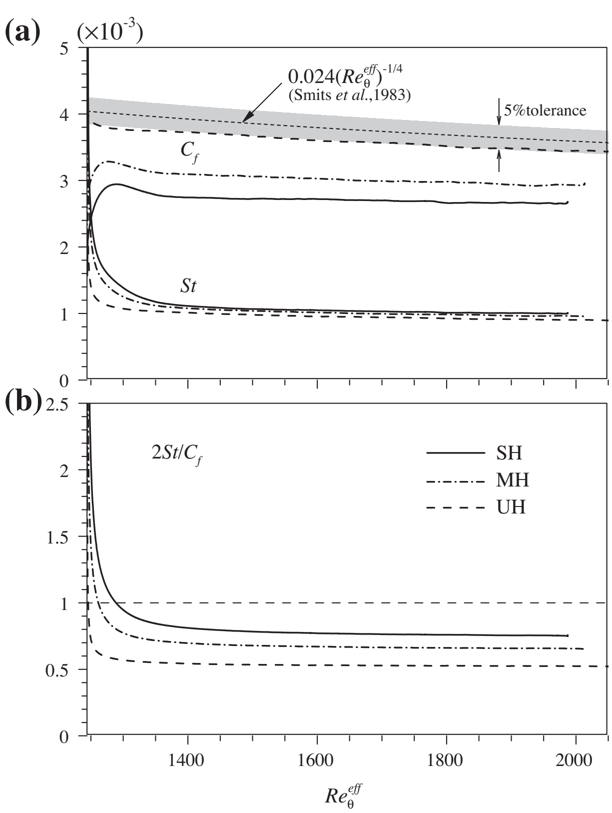

Fig. 1. Profiles of (a) the Stanton number (St) and the skin-friction coefficient (C_f) along the effective Reynolds number. (b) The Reynolds analogy factor ($2St/C_f$). (See above-mentioned references for further information.)

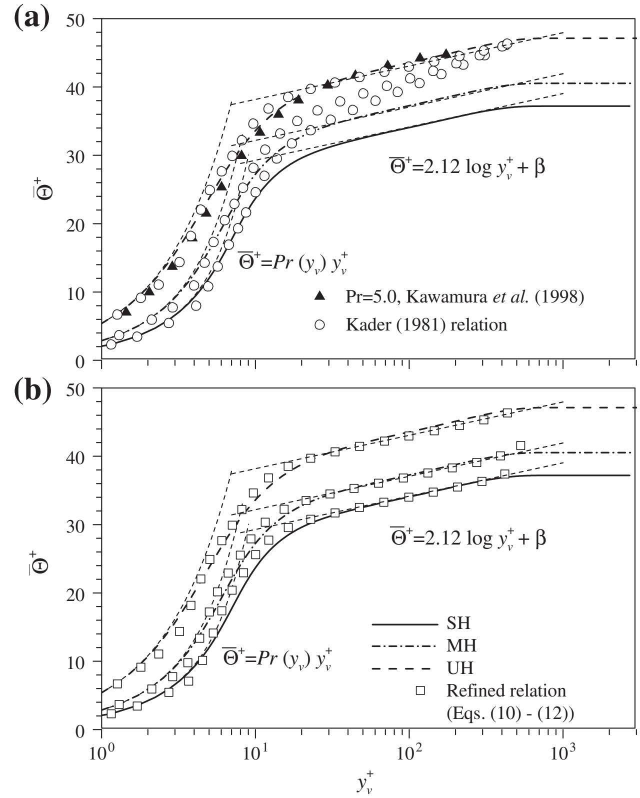

Fig. 2. Wall-normal distribution of mean scalar at $Re_\theta^{eff} = 1840$. Each profile is normalized by the friction temperature (Θ_τ) of each case. (a) Circle symbols (○) are the original relation of Kader (1981) and (b) square symbols (□) are the refined relation for the non-uniform Pr.

where

$$\beta(Pr) = (3.85Pr^{1/3} - 1.3)^2 + 2.13\ \ln\ Pr \tag{8}$$

and

$$\Gamma = \frac{0.01(Pr\ y^+)^4}{1 + 5Pr^3 y^+}. \tag{9}$$

Using this relation for $\bar{\Theta}^+(y; Pr)$, the wall-normal distribution of the mean scalar was evaluated and is plotted in Fig. 2a. Although the constant Prandtl number Pr in the original relation by Kader (Eqs. (7)–(9)) was replaced by the local value, $Pr(y)$, appreciable disagreement with the present DNS results is still observed in the outer region. In that region, the Prandtl number affects the wall-normal elevation β, which dictates the difference in the mean scalar between the wall and the lower edge of the log region (Kader, 1981). The disagreement originates from $\beta(Pr)$. In order to match the relation of the mean scalar and the present DNS results for a flow with temperature-dependent viscosity, we suggest a new β,

$$\beta(Pr_v) = (3.85Pr_v^{1/3} - 1.3)^2 + 2.13\ \ln\ Pr_v. \tag{10}$$

Because β denotes the wall-normal elevation of the log-law (dotted line in Fig. 2), β should be constant irrespective of y_v. In the work by Kader (1981), the log-law is valid for $30 < y^+ < \delta^+$ when $Pr \sim 1$, and therefore β is determined from $Pr_v \equiv Pr(y_v^+ = 30)$. Except for the definition of β, all Pr of the original relation by Kader(1981) should be replaced by the local value, $Pr(y)$, in order to reflect the local thermal behavior. Then, a refined scalar profile is obtained as,

$$\bar{\Theta}^+ = \underbrace{Pr(y) y_v^+ \exp(-\Gamma)}_{\text{inner}} + \underbrace{\left(2.12\ \ln\left((1+y_v^+)\frac{2.5(2-y/\delta)}{1+4(1-y/\delta)^2}\right) + \beta(Pr_v)\right)\exp(-1/\Gamma)}_{\text{outer}}, \tag{11}$$

where

$$\Gamma = \frac{0.01\left(Pr(y) y_v^+\right)^4}{1 + 5Pr(y)^3 y_v^+}. \tag{12}$$

Using the refined relation, we obtain an excellent agreement with the DNS data (see Fig. 2b). This implies that the modified inner length-scale (y_v^+) and the use of Pr_v are appropriate for capturing the mean scalar profile in the case of inhomogeneous Prandtl number. The refined mean scalar relation demonstrates that the law-of-the-wall in the conductive sublayer is governed by the local Prandtl number $Pr(y)$, and that the elevation of the log-law is determined by Prandtl number Pr_v at the start of the log region, near $y_v^+ = 30$.

3.1.2. Scalar fluctuations and scalar flux

The root-mean-square (r.m.s.) of the scalar fluctuations (Θ') is reported in Fig. 3, normalized by the friction temperature. The UH profile is in good agreement with that by Kawamura et al. (1998). Due to the isothermal wall boundary condition, the r.m.s. values of all cases approach zero at the wall. According to Tiselj et al. (2001) and Li et al. (2009), a decrease in Pr leads to a decrease in the r.m.s. of the scalar fluctuations (Θ'^+_{rms}) near the wall. While those studies were concerned with constant Pr flows, the trend is still preserved in the heated flow cases. The r.m.s. values of the scalar near the wall, including the peak value, all decrease in the case of temperature-dependent viscosity, where $Pr(y)$ is reduced. The peak position shifts from $y_v^+ = 6.39$ (UH) to $y_v^+ = 8.70$ (SH). Unlike the mean scalar profiles (Fig. 2), the r.m.s. profiles collapse in the outer region. However, the r.m.s. profiles show a significant deviation in the inner region even when normalized by Θ_τ (Fig. 3a). This dependence is due to the variation in the Prandtl number. The appropriate scaling of the profiles in the near-wall region is empirically obtained and is shown in Fig. 3b. In that figure, the r.m.s. values are normalized by $Pr(y)^{0.4}Pr_\infty^{0.15}$ and plotted against $Pr(y)^{0.5}y_v^+$. In summary, appropriate scaling for both the mean and r.m.s. profiles of the scalar fields have been constructed using the modified inner length-scale and the local Prandtl number.

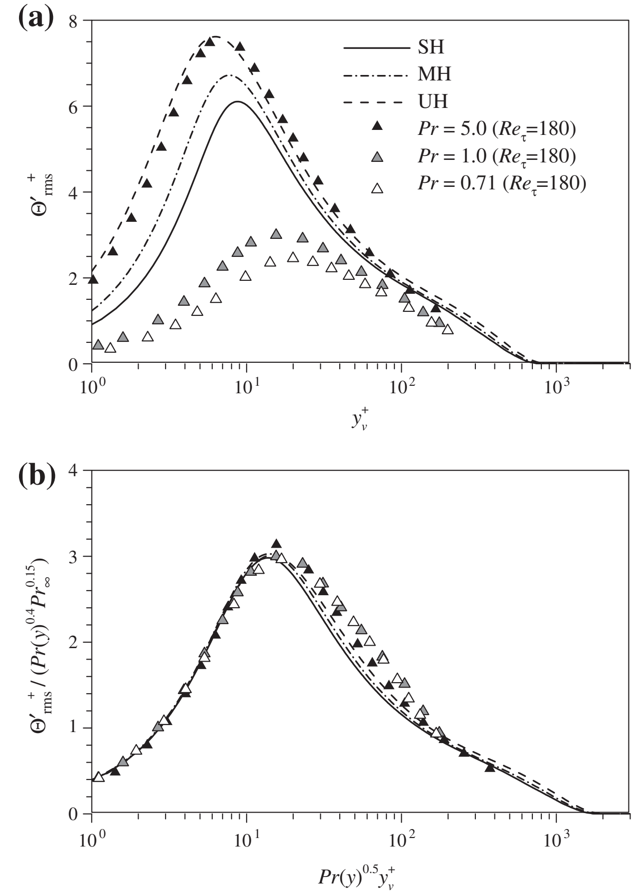

Fig. 3. Wall-normal distribution of r.m.s. of scalar fluctuation normalized by (a) the friction temperature (Θ_τ) and (b) both the friction temperature (Θ_τ) and the Prandtl numbers ($Pr(y)$ and Pr_∞) at $Re_\theta^{eff} = 1840$. All triangle symbols (▲) represent the scalar fluctuations in channel flow (Kawamura et al., 1998).

Profiles of the scalar fluxes $\overline{u_i'\Theta'}$ are shown in Fig. 4. When the inflow quantities U_∞, Θ_∞ and θ_{in} are used as reference scales (Fig. 4a), both the streamwise and wall-normal scalar fluxes for the MH and SH cases increase near the heated wall. Note that the r.m.s. of the scalar fluctuations in the reference scaling ($\Theta'_{rms}/\Theta_\infty$) are almost identical near the wall (not shown), and the field behavior of $\overline{u'\Theta'}$ at small y reflects changes in the streamwise velocity fluctuation. Using the inner scaling based on the friction quantities and l_v (Fig. 4b), the trend increases and follows the trend of Θ'^+_{rms} previously shown in Fig. 3a: Both the streamwise and wall-normal scalar fluxes for the temperature-dependent viscosity decrease near the wall. While this inner scaling collapses the r.m.s. velocity fluctuations (see Fig. 5d of Lee et al., 2013), it is not adequate for the scalar fluctuations (Fig. 3a) or their fluxes (Fig. 4b). The decrease of the scalar flux originates from the weakened scalar fluctuations (Fig. 3a). Note, however, that the near-wall slopes are 2 and 3 for $\overline{u'\Theta'}$ and $\overline{v'\Theta'}$, respectively, which are the same values as those reported in the literature at constant viscosity, i.e. constant Pr, (Kong et al., 2000).

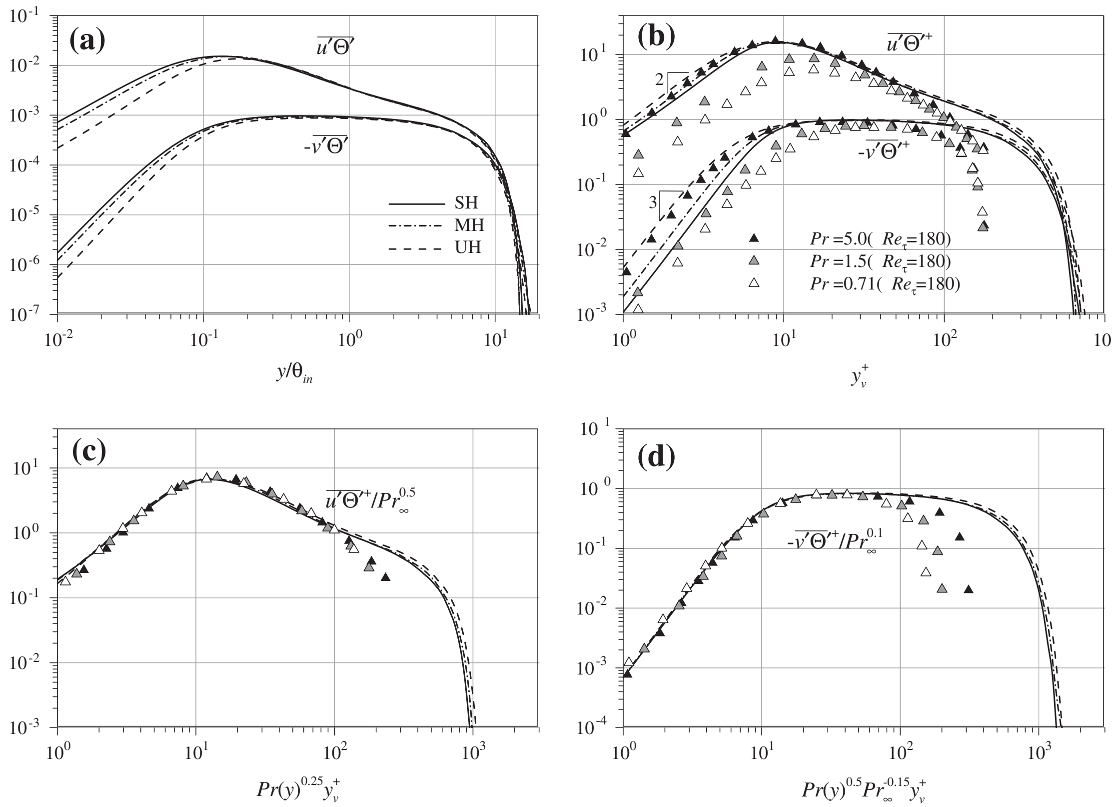

Fig. 4. Wall-normal distributions of scalar flux ($\overline{u_i'\Theta'}$) at $Re_\theta^{eff} = 1840$. Independent variables scaled by (a) the inlet momentum thickness (θ_{in}); (b) the modified inner-length scale (l_v); (c) $Pr(y)^{0.25}$ and l_v; (d) $Pr(y)^{0.5}Pr_\infty^{-0.15}$ and l_v. Dependent variables scaled by (a) the free-stream velocity (U_∞) and scalar (Θ_∞); (b) the friction velocity (u_τ) and scalar (Θ_τ); (c) u_τ, Θ_τ and $Pr_\infty^{0.5}$; (d) u_τ, Θ_τ and $Pr_\infty^{0.1}$. All triangle symbols (▲) represent the scalar fluctuations of channel flows (Kawamura et al., 1998).

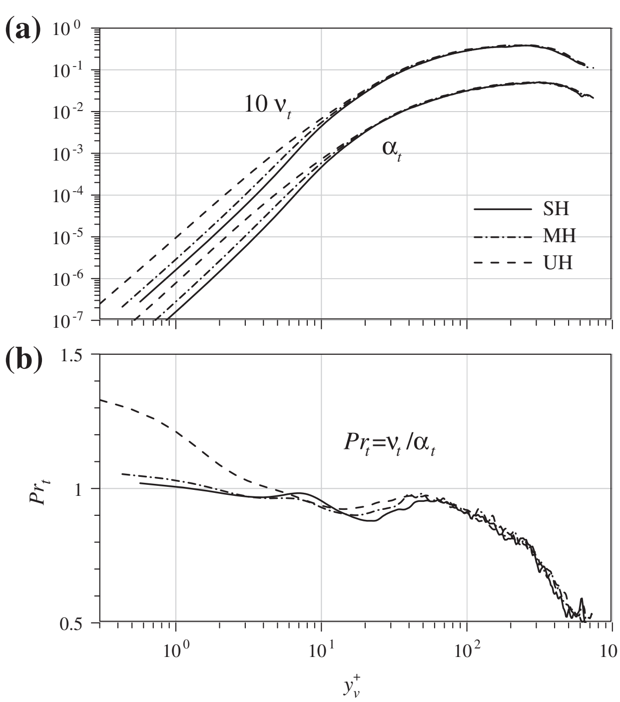

Fig. 5. Wall-normal distributions of (a) the turbulent eddy viscosity (ν_t) and the turbulent eddy diffusivity (α_t). (b) Wall-normal distributions of the turbulent Prandtl number at $Re_\theta^{eff} = 1840$.

Similar to the profiles of the r.m.s. scalar fluctuations, the profiles of the fluxes can be plotted using the modified inner length-scale and the local Prandtl number. Since the locations of the peak values of the fluxes are almost identical in all cases (see UH, MH and SH cases and data by Kawamura et al. (1998) at $Pr = 5.0$ in Fig. 4b), an appropriate near-wall scaling can be obtained using $Pr(y)$ and $l_v(y)$ because the thermal layer is thin relative to the momentum boundary layer. In addition, the scaling must take into account the effect of Pr_∞, which shows large fluxes for large Pr_∞ (Kawamura et al., 1998; Li et al., 2009). Therefore, the appropriate scaling is finally obtained using Pr_∞, $Pr(y)$ and $l_v(y)$. The outcome is shown in Fig. 4c and d. The profiles of the streamwise scalar flux (Fig. 4c) normalized by $Pr_\infty^{0.5}$ collapse well with $Pr(y)^{0.25}$ and $l_v(y)$. The wall-normal scalar flux normalized by $Pr_\infty^{0.1}$ is plotted against the scaled coordinate $Pr(y)^{0.5}Pr_\infty^{-0.15}y_v^+$ in Fig. 4d. This proposed scaling is in good agreement with both variable-viscosity flows (MH and SH) and the reference calculation of constant Prandtl number (UH). In addition, the scaling also collapses the data by Kawamura et al. (1998) for different Pr_∞ in the near-wall region.

3.1.3. Turbulent Prandtl number

The turbulent Prandtl number is a key concept in the development of turbulence models for scalar transport in bounded shear flows (Kong et al., 2000). To compute the turbulent Prandtl number, the turbulent eddy viscosity ($\nu_t \equiv -\overline{u'v'}/(\partial U/\partial y)$) and the turbulent eddy diffusivity ($\alpha_t \equiv -\overline{v'\Theta'}/(\partial\bar{\Theta}/\partial y)$) are obtained and reported in Fig. 5a. Due to the isothermal boundary condition, both ν_t and α_t are proportional to y^3 near the wall. The increase of $\partial U/\partial y$ near the wall is most dominant relative to the other terms in the definitions of α_t and ν_t, namely $\partial\bar{\Theta}/\partial y, \overline{u'v'}$ and $\overline{\Theta'v'}$. The turbulent Prandtl number $Pr_t \equiv \nu_t/\alpha_t$ is shown in Fig. 5b. As the viscosity difference increases, the near-wall Pr_t decreases. In all cases, Pr_t decreases with increasing wall-normal distance in the range $y_v^+ < 15$. A small peak around $y_v^+ \approx 50$ is observed, in agreement with previous studies (Kong et al., 2000; Li et al., 2009).

The asymptotic near-wall behavior of Pr_t is derived below. Similar to previous studies (Antonia and Kim, 1991; Na and Hanratty, 2000; Kong et al., 2000), ν_t and α_t are expressed in terms of polynomials. Following Na and Hanratty (2000), a fifth-order polynomial is adopted,

$$\alpha_t/y^3 = a_0 + a_1 y + a_2 y^2 + O(y^3), \tag{13}$$

and

$$\nu_t/y^3 = n_0 + n_1 y + n_2 y^2 + O(y^3). \tag{14}$$

The limiting behavior of the turbulent eddy viscosity and diffusivity normalized by y^3 is shown in Fig. 6. In the $y \to 0$ limit, $Pr_t = n_0/a_0$ (see details in Table 4). The maximum value (wall-asymptotic value) in the UH case is 1.41 at the wall. This value is larger than that reported by Kong et al. (2000) ($Pr_t = 1.1$ for $Pr = 0.71$ and $Re_\theta = 300$) and Li et al. (2009) ($Pr_t = 1.1$ for any Pr lower than 2.0 and $Re_\theta = 830$), which is consistent due to the higher Pr in the current UH case ($Pr = 5.4$). The maximum value of Pr_t decreases to 1.08 and 1.03 in the MH and SH flows. This drop is consistent with the decreased local Pr near the heated surface. The lower values of Pr_t within the current Pr-range is in a good agreement with Kozuka et al. (2009). Note that $Pr_t = 1.03$ in the SH case can be regarded to approach the lower-most value at $Re_\theta^{eff} = 1840$, because the SH case represents the near boiling temperature of water ($T_w = 99$ °C). The herein reported increase in the Reynolds analogy factor towards unity (Fig. 1b) is consistent with the decreased Pr_t ($Pr_t \to 1$) in the present viscosity model. This effectively implies that the scalar transport is augmented due to fluid motions. Thus, consideration of the viscosity variation with temperature is critical to prediction of the thermal field at large temperature differences.

3.2. Scalar transport

3.2.1. Contributions to the Stanton number

As shown in Fig. 1a, the temperature-dependent viscosity leads to an increase in the Reynolds analogy factor ($2St/C_f$) and the scalar transfer coefficient (St). The wall-normal gradient of the mean scalar normalized by Θ_∞ and θ_{in} increases in the SH case (not shown), which leads to the enhanced scalar transport near the wall. Although the increase in St is synonymous with the increase in the mean scalar gradient, the variation of the gradient is caused by the action of turbulent thermal events throughout the entire boundary layer. This relationship is examined in detail in this section.

Table 4
Limiting values of the turbulent eddy viscosity (ν_t/y^3) and the turbulent eddy diffusivity (α_t/y^3) near the wall.

	a_0	a_1	a_2	n_0	n_1	n_2
Constant viscosity (UH)	0.0804	1.12	−7.13	0.114	0.418	−4.07
Moderately heated (MH)	0.184	1.08	−18.7	0.198	0.242	−10.2
Strongly heated (SH)	0.257	0.717	−25.2	0.266	−0.222	−12.6

Fukagata et al. (2002) proposed an approach to identify various contributions to the skin-friction coefficient. They performed wall-normal integration of the Reynolds-averaged Navier-Stokes (RANS) equation for the streamwise momentum, and obtained an identity for the skin-friction coefficient. This identity can be instructive in the analysis of the origin of changes to the skin-friction. Here, a similar approach is adopted for the energy equation in variable-viscosity flows,

$$\begin{aligned} St_{identity} = & \underbrace{\frac{2}{\delta^2 Re_{\theta_{in}} Pr}\int_0^\delta \bar{\Theta} dy}_{St(\Theta)} + \underbrace{\frac{2}{\delta^2 Re_{\theta_{in}} Pr}\int_0^\delta (\delta - y)^2 \frac{\partial^2 \bar{\Theta}}{\partial x^2} dy}_{St(\partial^2\Theta/\partial x^2)} \\ & \underbrace{-\frac{1}{\delta^2}\int_0^\delta (\delta - y)^2 \frac{\partial}{\partial x}(U\bar{\Theta}) dy}_{(i) St(U\Theta)} \underbrace{- \frac{2}{\delta^2}\int_0^\delta (\delta - y) V \bar{\Theta} dy}_{(ii) St(V\Theta)} \\ & \underbrace{-\frac{2}{\delta^2}\int_0^\delta (\delta - y)\overline{v'\Theta'} dy}_{(iii) St(v'\Theta')} \underbrace{- \frac{1}{\delta^2}\int_0^\delta (\delta - y)^2 \frac{\partial}{\partial x}\left(\overline{u'\Theta'}\right) dy}_{St(u'\Theta')}. \end{aligned} \tag{15}$$

In Eq. (15), the first and second terms on the right-hand side are related to the mean scalar; the third and fourth terms are related to the mean scalar fluxes; and the last two terms are related to the turbulent scalar fluxes. The Stanton numbers evaluated from the mean scalar profile and from the above expression are plotted in Fig. 7 versus the effective Reynolds number. The result from the identity ($St_{identity}$) is in excellent agreement with the original definition (St). The various contributions to the Stanton number (Eq. (15)) are shown in Fig. 8a. The results demonstrate that three terms are important, namely (i) the streamwise gradient of $U\bar{\Theta}$ denoted $St(U\Theta)$; (ii) the product of the mean wall-normal velocity and scalar $St(V\Theta)$; and (iii) the correlation between the wall-normal

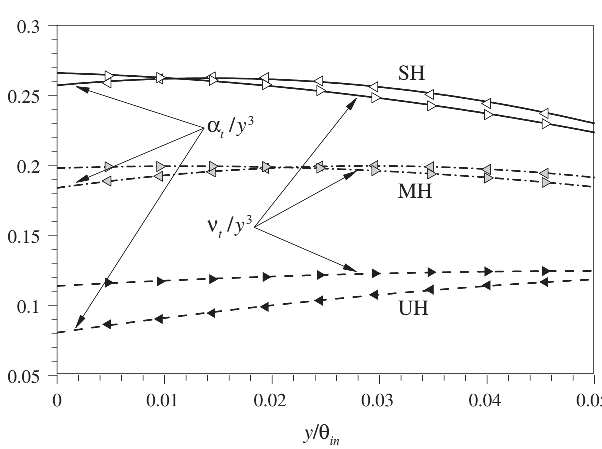

Fig. 6. Limiting behavior of the turbulent eddy viscosity (ν_t/y^3) and the turbulent eddy diffusivity (α_t/y^3) near the wall. Symbols indicate the positions of the grid points. Lines represent the polynomial fit with an order of 2.

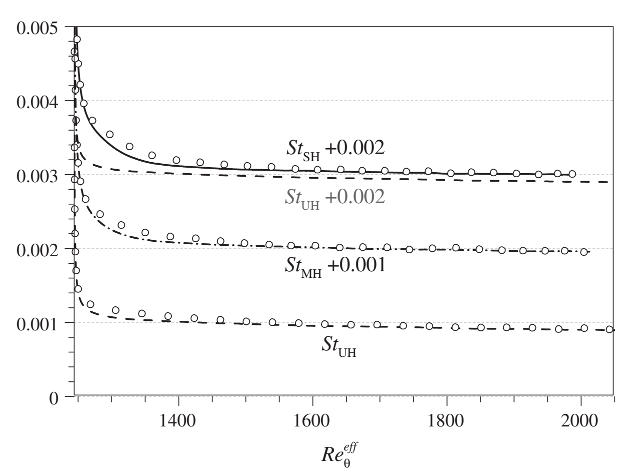

Fig. 7. Stanton numbers, computed from the mean scalar gradient St (lines) and from the identity $St_{identity}$ (symbols) as a function of the effective Reynolds number.

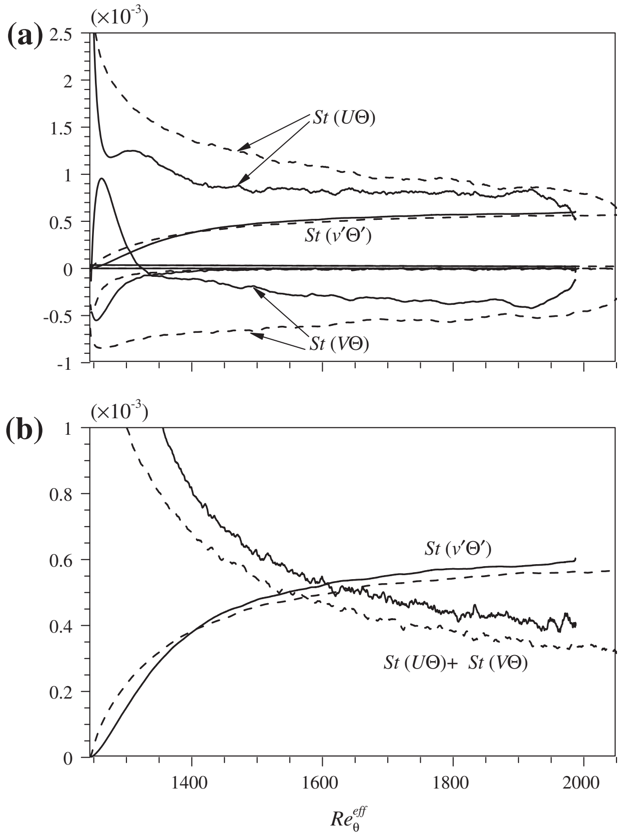

Fig. 8. Contributions to the Stanton number. Solid and dashed lines indicate SH and UH, respectively. (a) All St-identity terms and (b) only $St(v'\Theta')$ and $St(U\Theta)+St(V\Theta)$ terms.

velocity fluctuation and scalar fluctuation $St(v'\Theta')$. The remaining terms make a contribution near the inlet only, where the isothermal heating starts, and become vanishingly small downstream of $Re_\theta^{eff}=1400$.

The most significant contributions to the change in the Stanton number in the heated flow can be attributed to terms (i) $St(U\Theta)$ and (ii) $St(V\Theta)$. The former, (i) $St(U\Theta)$, has an unfavorable effect, i.e. it reduces the Stanton number, and is attributed to the reduction in the growth rate of the boundary layer in the heated flow. The second term, (ii) $St(V\Theta)$, contributes favorably to the change in the Stanton number, and is a result of the reduction in the displacement thickness (Lee et al., 2013). These two terms should therefore be viewed together, and their net contribution is plotted in Fig. 8b. Their net effect is an increase in the Stanton number. The figure also shows the wall-normal scalar flux, (iii) $St(v'\Theta')$, which has a comparable change relative to the change in $St(U\Theta)+St(V\Theta)$. For example, the 10.4% increase in the Stanton number at $Re_\theta^{eff}=1840$ is due to 7.7% increase in $St(U\Theta)+St(V\Theta)$ and a 2.7% increase in $St(v'\Theta')$. Note also that the modification of $-\overline{v'\Theta'}$ is most pronounced near the wall (Fig. 4a), where changes in the mean flow are appreciable. This motivates a closer examination of the turbulent scalar flux with particular attention to the near-wall region.

3.2.2. Scalar flux budget

In this section, the transport equation for the scalar flux is evaluated. Because the viscosity in the momentum equation is dependent on temperature, corresponding terms appear in the averaged scalar flux equation,

$$0=\underbrace{-U_j\frac{\partial\overline{u_i'\Theta'}}{\partial x_j}}_{C_{\Theta,i}}\underbrace{-\overline{u_j'\Theta'}\frac{\partial U_i}{\partial x_j}-\overline{u_i'u_j'}\frac{\partial\bar{\Theta}}{\partial x_j}}_{P_{\Theta,i}}+\underbrace{\overline{p'\frac{\partial\Theta'}{\partial x_i}}}_{\Pi_{\Theta,i}}\underbrace{-\frac{\partial\overline{p'\Theta'}}{\partial x_i}}_{G_{\Theta,i}}\underbrace{-\frac{\partial\overline{u_i'u_j'\Theta'}}{\partial x_j}}_{T_{\Theta,i}}$$
$$+\underbrace{\frac{\partial}{\partial x_j}\left(\frac{1}{Pe}\overline{u_i'\frac{\partial\Theta'}{\partial x_j}}+\frac{1}{Re}\overline{\Theta'\frac{\partial u_i'}{\partial x_j}}\right)}_{D_{\Theta,i}}-\underbrace{\left(\frac{1}{Re}+\frac{1}{Pe}\right)\overline{\frac{\partial u_i'}{\partial x_j}\frac{\partial\Theta'}{\partial x_j}}}_{\varepsilon_{\Theta,i}}$$
$$+VS1_{\Theta,i}+VS2_{\Theta,i}+VS3_{\Theta,i}+VS4_{\Theta,i}+VS5_{\Theta,i}. \tag{16}$$

In the above budget, $C_{\Theta,i}$ denotes convection, $P_{\Theta,i}$ is production, $\Pi_{\Theta,i}+G_{\Theta,i}$ are terms involving the velocity–pressure-gradient correlation, $T_{\Theta,i}$ is the turbulent transport, $D_{\Theta,i}$ the viscous diffusion, and $\varepsilon_{\Theta,i}$ is the dissipation. The additional viscosity stratification (VS_Θ) terms are:

$$VS1_{\Theta,i}=\frac{2}{Re}\frac{\partial\overline{v_R}}{\partial x_j}\overline{\Theta's_{ij}}, \tag{17}$$

$$VS2_{\Theta,i}=\frac{2}{Re}S_{ij}\overline{\Theta'\frac{\partial v_R'}{\partial x_j}}, \tag{18}$$

$$VS3_{\Theta,i}=\frac{2}{Re}\overline{s_{ij}\Theta'\frac{\partial v_R'}{\partial x_j}}, \tag{19}$$

$$VS4_{\Theta,i}=\frac{1}{Re}\overline{\Theta'v_R'}\frac{\partial^2U_i}{\partial x_j^2}, \tag{20}$$

$$VS5_{\Theta,i}=\frac{1}{Re}\overline{\Theta'v_R'\frac{\partial^2u_i'}{\partial x_j^2}}, \tag{21}$$

where $S_{ij}=\frac{1}{2}\left(\frac{\partial U_i}{\partial x_j}+\frac{\partial U_j}{\partial x_i}\right)$ and $s_{ij}=\frac{1}{2}\left(\frac{\partial u_i'}{\partial x_j}+\frac{\partial u_j'}{\partial x_i}\right)$.

The budgets of the scalar flux for the UH and SH cases are compared in Fig. 9. The scaling of the wall-normal coordinate ($Pr^{0.25}y^+$) by Li et al. (2009) is modified to take into account the local Pr, i.e. $Pr(y)^{0.25}y_v^+$. In order to assess the effect of introducing the wall heating downstream of the inlet, all the budget terms are normalized by $U_\infty^2\Theta_\infty/\theta_{in}$. In the profiles of the budget for $\overline{u'\Theta'}$ (Fig. 9a), the production term increases in the buffer region. Similar to the TKE budget, the production and the viscous diffusion terms are the largest in the buffer layer and in the viscous sublayer, respectively. The peak value of the production increases for the heated flow. Here, the production term for $\overline{u'\Theta'}$ is:

$$P_{\Theta,1}=-\overline{u'\Theta'}\frac{\partial U}{\partial x}-\overline{v'\Theta'}\frac{\partial U}{\partial y}-\overline{u'u'}\frac{\partial\bar{\Theta}}{\partial x}-\overline{u'v'}\frac{\partial\bar{\Theta}}{\partial y}. \tag{22}$$

The increase of the peak value results from the 2nd and 4th terms in Eq. (22), because the remaining terms are negligible given the relatively small value of the mean streamwise gradients in comparison to the wall-normal gradients. Even though the values of $-\overline{v'\Theta'}$ and $-\overline{u'v'}$ are only slightly changed in the sublayer and buffer regions for the heated flow, those of $\partial U/\partial y$ and $\partial\bar{\Theta}/\partial y$ are significantly increased in these regions. The increased wall-normal gradients are mainly responsible for the large production in the heated flow.

Near the wall, the viscous diffusion term decreases and the dissipation term increases. The changes in the viscous diffusion and the dissipation are balanced by the $VS_{\Theta,i}$ term ($VS_{\Theta,i}=VS1_{\Theta,i}+VS2_{\Theta,i}+VS3_{\Theta,i}+VS4_{\Theta,i}+VS5_{\Theta,i}$). The enhanced dissipation in the sublayer is required to balance the diffusion and VS_Θ terms at the wall. In terms of turbulent structures, the enhanced dissipation is established by a reduction in the smallest scales in the low-viscosity, near-wall layer (Lee et al., 2013). The sum of the viscosity

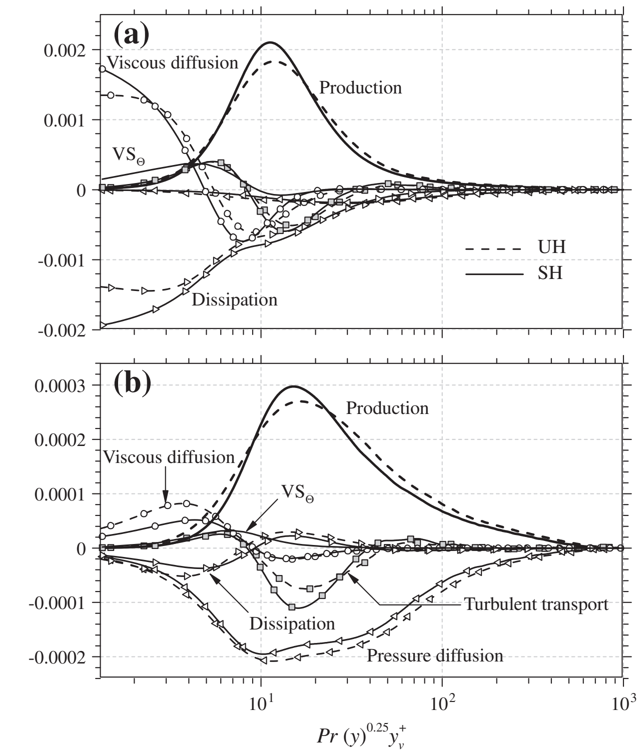

Fig. 9. Budgets of (a) streamwise scalar flux $\overline{u'\Theta'}$ and (b) wall-normal scalar flux $-\overline{v'\Theta'}$ at $Re_\theta^{eff} = 1840$. Every term is normalized by $U_\infty^2 \Theta_\infty/\theta_{in}$.

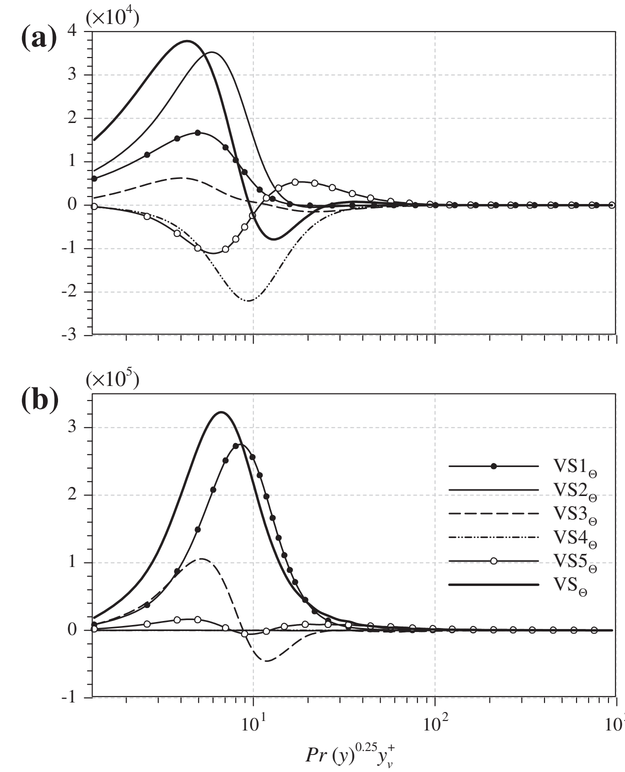

Fig. 10. Additional $VS_{\Theta,i}$ terms of SH at $Re_\theta^{eff} = 1840$. Every term is normalized by $U_\infty^2 \Theta_\infty/\theta_{in}$. (a) The streamwise $\overline{u'\Theta'}$ and (b) the wall-normal flux $-\overline{v'\Theta'}$, respectively.

stratification terms is a gain in the sublayer and a loss near the production peak, which mimics the effect of the viscous diffusion.

The budget of the wall-normal scalar flux $-\overline{v'\Theta'}$ is shown in Fig. 9b. The peak value of the production term is increased due to the large wall-normal gradient of the mean scalar. The sum of the $VS_{\Theta,i}$ terms appears as a gain term. While the change in pressure diffusion (the dominant loss term) by wall heating is negligible, the dissipation and turbulent transport terms are changed to a greater extent: The dissipation decreases in the sublayer and the turbulent transport increases in the buffer region, respectively. To balance with the lower dissipation in the sublayer, the viscous diffusion term decreases. This figure demonstrates that transport of the wall-normal scalar flux is reduced between the location of its peak and the wall in the variable viscosity flow.

Fig. 10 displays the additional $VS_{\Theta,i}$ terms in the SH case. In both the streamwise and wall-normal scalar fluxes, the $VS1_{\Theta,i}$ term, which reflects the wall-normal gradient of the mean viscosity ratio ($\bar{\nu}_R$), has the largest contribution. Most of the viscosity stratification effect is in the inner region, in particular $Pr(y)^{0.25} y_v^+ \simeq 30$. Overall, the $VS_{\Theta,i}$ terms play a role which is similar to viscous diffusion whereby the scalar flux is transported towards the wall.

3.3. Turbulent thermal structures

The statistics of the scalar field (Section 3.1) and of its fluxes (Section 3.2) are connected to the modification of turbulent thermal structures in the variable viscosity flow. Fig. 4a showed that the wall-normal scalar flux in the SH case increases in the near-wall region. A manifestation of this increase in terms of instantaneous structures is given in Fig. 11. The figure shows contours of the wall-normal scalar flux near the wall for both the reference and the heated flows. The large population density of near-wall vortical structures (grey) in the SH case corresponds to the enhanced fine-scale motions reported by Lee et al. (2013). Note that the crowded contour of the scalar flux is similar to the

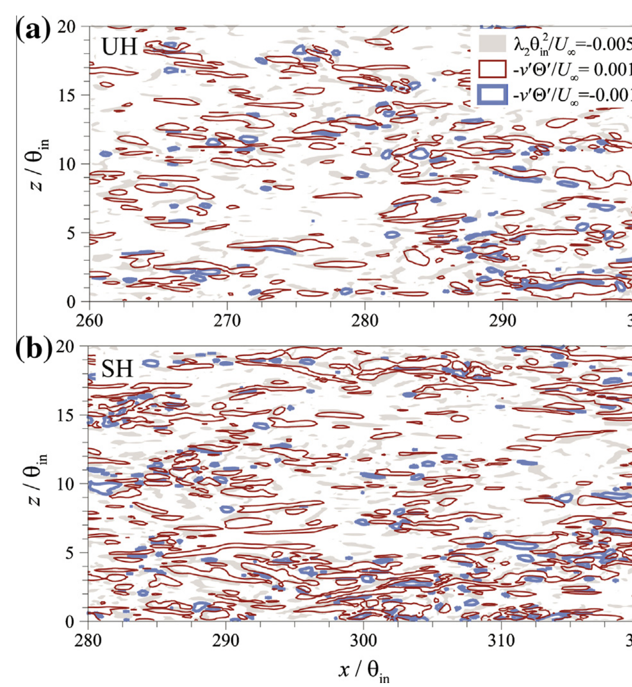

Fig. 11. Contours of the wall-normal scalar flux in the near-wall region $y/\theta_{in} = 0.11$ ($y^+ = 5.5$ of UH) using $-v'\Theta'/U_\infty = 0.001$ (red) and -0.001 (blue). (a) UH and (b) SH. Grey regions of vortical structures using $\lambda_2\theta_{in}^2/U_\infty^2 = -0.005$. (For interpretation of the references to colour in this figure legend, the reader is referred to the web version of this article.)

observation of surface heat-flux fluctuations in the large Reynolds-number flow by Abe et al. (2004). Because the quasi-streamwise vortices induce the wall-normal fluid motions, the position of the scalar flux is closely related to the position of the vortical structures. Positive regions of $-\overline{v'\Theta'}$ (red) are increased in the heated flow. However, negative regions of $-\overline{v'\Theta'}$ (blue) are nearly identical in both cases. Therefore, there is an overall increase in $-\overline{v'\Theta'}$ in the variable viscosity case, which contributes to the increase in the Stanton number via the term $St(v'\Theta')$.

The two-point correlation between the wall-normal velocity and scalar fluctuations, given by

$$R_{-v'\Theta'}(r_x, r_z) = \frac{\overline{-v'(x,z)\Theta'(x+r_x, z+r_z)}}{v'_{rms}\Theta'_{rms}}, \tag{23}$$

was evaluated to support the observations from the instantaneous flow fields. As shown in Fig. 12, the spatial extent of the positive correlation (high-temperature region for upward motion at the reference position; or low-temperature region for downward motion at the reference position) is increased in the downstream direction. Because the upward motions (ejection events) are more dominant in the sublayer, this indicates that high-temperature transport takes place in a wider region around the upward fluid motion at the reference position. The hot fluid parcels ($\Theta' < 0$) in the SH case convect further in the downstream direction by an enhanced mean streamwise velocity near the wall in the heated flow (Fig. 5a of Lee et al. (2013)). In addition, since the wall-normal velocity fluctuations are 52% higher than those of the UH case at $y/\theta_{in} = 0.11$ (not shown), Θ' is correlated with the strong v' in a wide area. The long positive region of the two-point correlation is similar to the appearance of long near-wall vortices in the SH case, because the ejection events reside along with the near-wall vortices (Fig. 11). In addition, the high population density of elongated vortices near the wall reflects the high local Reynolds number due to the local decrease in viscosity.

The negative regions of the correlation in Fig. 11 (upward motion of low temperature; or downward motion of high temperature at the reference position) are observed near the reference position. This is caused by a counter-balance of the wall-normal velocity fluctuations at the reference position. Both the spatial extent and the maximum value of the negative correlation are decreased in the heated flow.

Shaw and Hanratty (1977) showed that the high-frequency fluctuations in mass transfer are diminished with increasing Schmidt number. Later, Hasegawa and Kasagi (2009) reported the spatio-temporal correlation of fluctuations in velocity and concentration in order to quantify the reduction in the high-frequency in concentration fluctuations. They termed this behavior the low-pass filtering effect at high Schmidt number. Although the previous studies focused on the concentration fields and the

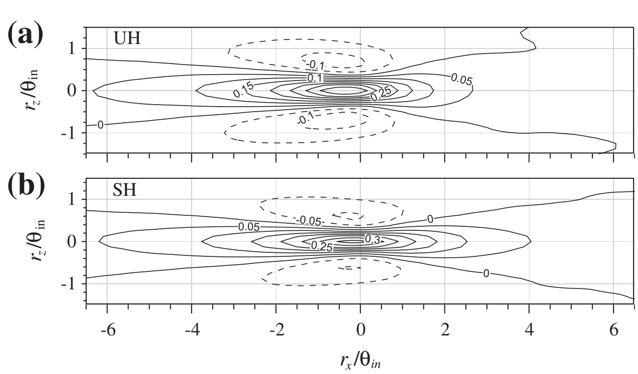

Fig. 12. Two-point correlation between the wall-normal velocity and the scalar fluctuations ($R_{-v'\Theta'}$) at $y/\theta_{in} = 0.11$ ($y^+ = 5.5$ of UH ($Re_\theta^{eff} = 1,840$)). (a) UH and (b) SH. Contour levels are from -0.1 to 0.4 with increments of 0.05.

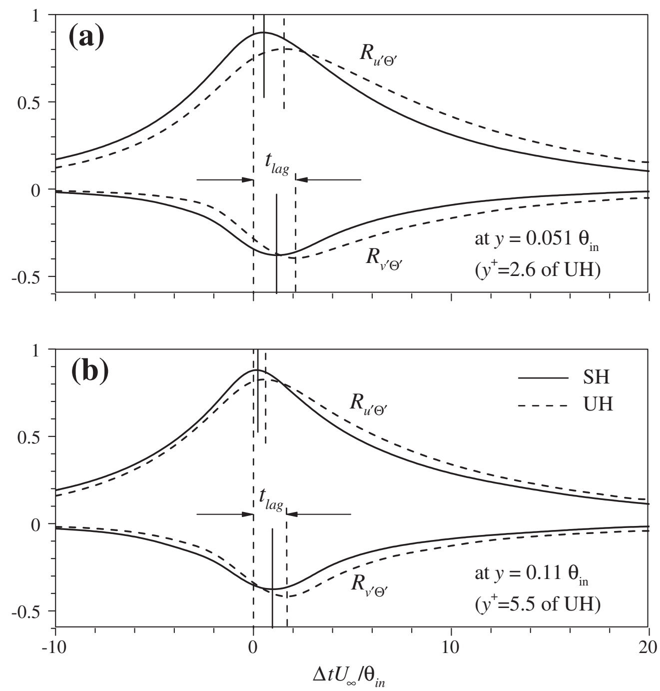

Fig. 13. Spatio-temporal correlation coefficient between the streamwise and the scalar fluctuations ($R_{u'\Theta'}$), and that between the wall-normal velocity and the scalar fluctuations ($R_{v'\Theta'}$) at $Re_\theta^{eff} = 1840$. (a) $y/\theta_{in} = 0.051$ ($y^+ = 2.6$ of UH) and (b) $y/\theta_{in} = 0.11$ ($y^+ = 5.5$ of UH).

high-Schmidt-number effect, the same low-pass filtering of fluctuations in the scalar is expected in high-Pr flows.

In the SH case, the vigorous fluctuations in the scalar flux inside the viscous sublayer can be regarded as a result of a weakening in the low-pass filtering. To assess the strength of the filtering effect, the spatio-temporal correlation of the velocity and scalar fluctuations ($R_{u_i'\Theta'}$) in the near-wall region is reported in Fig. 13. The correlation is defined as $R_{u_i'\Theta'}(\Delta t) = \overline{u_i'(t)\Theta'(t+\Delta t)}$ at the reference position, and is normalized by the r.m.s. of each event. There is a reduction in the time lag (t_{lag}) between the velocity and scalar fluctuations in the variable viscosity flow, where t_{lag} is defined as the duration from the reference time to the extremum of the correlation. For instance, the time lag is decreased by 34.5% ($R_{u'\Theta'}$) and 54.9% ($R_{v'\Theta'}$) at $y = 0.051\theta_{in}$. The reduction is 35.9% ($R_{u'\Theta'}$) and 56.1% ($R_{v'\Theta'}$) at $y = 0.11\theta_{in}$. The decreased time lag of the SH case indicates a weakening of the low-pass filtering effect. In other words, the high-frequency velocity signal affects the scalar fluctuations to a greater extent. The decreased time lag implies a rapid scalar transport from the heated wall, which is consistent with the low turbulent Prandtl number in the near-wall region. The near-wall behavior is closely related to the near-wall turbulence structures which become more energetic in the heated flow. This was shown by Lee et al. (2013) by comparing the premultiplied spanwise energy spectra of the u'-velocity and the joint probability density function of $Q_s(\equiv(S_{ij}S_{ji})/2)$ and $R_s(\equiv(S_{ij}S_{jk}S_{ki})/3)$ near the wall. Here, $S_{ij} = (\partial u_i/\partial x_j + \partial u_j/\partial x_i)/2$ is the symmetric component of the velocity gradient tensor (Blackburn et al., 1996; Ooi et al., 1999). The results by Lee et al. (2013) demonstrated that the small scales are more energetic near the wall in the heated flows. This leads to an abundance of high-frequency fluctuations of the scalar flux near the wall, which is consistent with the weakened low-pass filtering effect observed here. In summary, the large $-\overline{v'\Theta'}$ in the temperature-dependent viscosity flow stems from the large population of vortical structures (Fig. 11), and the greater extent of the two-point correlation $R_{-v'\Theta'}$ near the wall (Fig. 12). The swift response of Θ' to

v' events also favors, or enhances, the scalar flux near the heated wall. These combined effects lead to an enhanced contribution of turbulent motions to the scalar transport.

4. Summary and conclusions

The influence of wall-heating on turbulent thermal boundary layers with variable viscosity was investigated using DNS data. The fluid viscosity model was chosen to represent water at atmospheric pressure, and therefore lower viscosity at higher temperature. Based on two wall temperatures, moderately and strongly heated cases (MH and SH) were considered. A simulation with a conventional passive scalar approach (UH) was included for comparison. The present study focused on the effect of temperature-dependent viscosity on the statistics of both the scalar field and scalar transfer rate.

Due to the low near-wall viscosity in the heated flow, the Prandtl number reduces in that region. An associated increase in the friction temperature caused the statistics of the scalar field, such as the mean scalar, scalar fluctuation and scalar flux, to exhibit smaller values relative to the reference, isothermal flow. A unified relation for the mean scalar in the presence of inhomogeneous viscosity was proposed. In addition, appropriate scalings were presented for the scalar fluctuation and the scalar flux. The proposed functional form for the mean was based on the local and free-stream Prandtl numbers and the modified inner length-scale. It was also shown that the wall asymptotic value of the turbulent Prandtl number was reduced in the heated flow.

The combined effect of the reduction in skin-friction (Lee et al., 2013), and the increase in Stanton number (non-dimensional scalar transfer rate) leads to an increase in the Reynolds analogy factor by 44% in the variable viscosity flow relatively to the reference simulation. We derived an identity for the Stanton number to explain the effect of the variable viscosity on the scalar transfer rate. The individual terms in the identity indicated that the Stanton number is increased owing to the reduction in the mean wall-normal velocity and the increase in the wall-normal scalar flux. The change of the mean flow is a result of the reduction in the displacement thickness. The budget of the scalar flux showed that the peak value of the production is increased, owing to the large wall-normal gradients of the mean streamwise velocity and the mean scalar. The change in the scalar flux, $v'\Theta'$, was attributed to the modification of the turbulent thermal structures. In the viscous sublayer, a shorter lag was demonstrated in the response of the scalar fluctuations to the velocity fluctuations, which indicates a weakening of the low-pass filtering effect. Therefore, the wall-normal scalar flux was enhanced near the heated wall, which leads to a favorable contribution to the Stanton number.

In summary, the present findings showed that the temperature-dependence of fluid viscosity enhances heat transfer between the fluid and the wall. Combined with the previous findings by Lee et al. (2013), namely the reduction in turbulent drag, this work provides a complete description of turbulent liquid flow near a heated surface.

Acknowledgements

The authors would like to acknowledge the financial support from the Creative Research Initiatives program (No. 2014-001493) of the National Research Foundation of Korea (MSIP), and the financial and computing (HECToR) support from the UK Engineering and Physical Sciences Research Council (EPSRC).

References

Abe, H., Kawamura, H., Matsuo, Y., 2004. Surface heat-flux fluctuations in a turbulent channel flow up to $Re_\tau = 1020$ with $Pr = 0.025$ and 0.71. Int. J. Heat Fluid Fl. 25, 404–419.
Antonia, R.A., Kim, J., 1991. Turbulent Prandtl number in the near-wall region of a turbulent channel flow. Int. J. Heat Mass Transf. 34 (7), 1905–1908.
Blackburn, H.M., Mansour, N.N., Cantwell, B.J., 1996. Topology of fine-scale motions in turbulent channel flow. J. Fluid Mech. 310, 269–292.
Fukagata, K., Iwamoto, K., Kasagi, N., 2002. Contribution of Reynolds stress distribution to the skin friction in wall-bounded flows. Phys. Fluids 14, L73–L76.
Hasegawa, Y., Kasagi, N., 2009. Low-pass filtering effects of viscous sublayer on high Schmidt number mass transfer close to a solid wall. Int. J. Heat Fluid Fl. 30, 525–533.
Kader, B.A., 1981. Temperature and concentration profiles in fully-turbulent boundary layers. Int. J. Heat Mass Transf. 24, 1541–1544.
Kawamura, H., Ohsaka, K., Abe, H., Yamamoto, K., 1998. DNS of turbulent heat transfer in channel flow with low to medium-high Prandtl number fluid. Int. J. Heat Fluid Fl. 19, 482–491.
Kong, H., Choi, H., Lee, J.S., 2000. Direct numerical simulation of turbulent thermal boundary layers. Phys. Fluids 12, 2555–2568.
Kozuka, M., Seki, Y., Kawamura, H., 2009. DNS of turbulent heat transfer in a channel flow with a high spatial resolution. Int. J. Heat Fluid Fl. 30, 514–524.
Lee, J., Jung, S.Y., Sung, H.J., Zaki, T.A., 2013. Effect of wall heating on turbulent boundary layers with temperature-dependent viscosity. J. Fluid Mech. 726, 196–225.
Li, Q., Schlatter, P., Brandt, L., Henningson, D.S., 2009. DNS of a spatially developing turbulent boundary layer with passive-scalar transport. Int. J. Heat Fluid Fl. 30, 916–929.
Na, Y., Hanratty, T.J., 2000. Limiting behavior of tubulent scalar transport close to a wall. Int. J. Heat Mass Transf. 43, 1749–1758.
Nolan, K.P., Zaki, T.A., 2013. Conditional sampling of transitional boundary layers in pressure gradients. J. Fluid Mech. 43, 1749–1758.
Ooi, A., Martin, J., Soria, J., Chong, M.S., 1999. A study of the evolution and characteristics of the invariants of the velocity-gradient tensor in isotropic turbulence. J. Fluid Mech. 381, 141–174.
Sameen, A., Govindarajan, R., 2007. The effect of wall heating on instability of channel flow. J. Fluid Mech. 577, 417–442.
Shaw, D.A., Hanratty, T., 1977. Influnce of Schmidt number on the fluctuations of turbulent mass transfer to a wall. AIChE J. 23 (2), 160–169.
Smits, A.J., Matheson, N., Joubert, P.N., 1983. Low-Reynolds-number turbulent boundary layers in zero and favourable pressure gradients. J. Ship Res. 27, 147–157.
Tiselj, I., Pogrebnyak, E., Li, C., Mosyak, A., Hetsroni, G., 2001. Effect of wall boundary condition on scalar transfer in a fully developed turbulent flume. Phys. Fluids 13, 1028–1039.
Wall, D.P., Wilson, S.K., 1997. The linear stability of flat-plate boundary-layer flow of fluid with temperature-dependent viscosity. Phys. Fluids 9, 2885–2898.
White, F.M., 2006. Viscous Fluid Flow, Third ed.. McGraw-Hill.
Wu, X., Moin, P., 2010. Transitional and turbulent boundary layer with heat transfer. Phys. Fluids 22, 085105.
Zaki, T.A., 2013. From streaks to spots and on to turbulence: exploring the dynamics of boundary layer transition. Flow Turbul. Combust. 91, 451–473.
Zaki, T.A., Wissink, J.G., Rodi, W., Durbin, P.A., 2010. Direct numerical simulations of transition in a compressor cascade: the influence of free-stream turbulence. J. Fluid Mech. 665, 57–98.
Zonta, F., Marchioli, C., Soldati, A., 2012. Modulation of turbulence in forced convection by temperature-dependent viscosity. J. Fluid Mech. 697, 150–174.